

# Nanoscale

Accepted Manuscript



This is an *Accepted Manuscript*, which has been through the Royal Society of Chemistry peer review process and has been accepted for publication.

*Accepted Manuscripts* are published online shortly after acceptance, before technical editing, formatting and proof reading. Using this free service, authors can make their results available to the community, in citable form, before we publish the edited article. We will replace this *Accepted Manuscript* with the edited and formatted *Advance Article* as soon as it is available.

You can find more information about *Accepted Manuscripts* in the [Information for Authors](#).

Please note that technical editing may introduce minor changes to the text and/or graphics, which may alter content. The journal's standard [Terms & Conditions](#) and the [Ethical guidelines](#) still apply. In no event shall the Royal Society of Chemistry be held responsible for any errors or omissions in this *Accepted Manuscript* or any consequences arising from the use of any information it contains.



Cite this: DOI: 10.1039/xxxxxxxxxx

## Morphology and local conductance of single crystalline Bi<sub>2</sub>Te<sub>3</sub> thin films on mica

R. Rapacz,<sup>a,b</sup> K. Balin<sup>a,b</sup>, M. Wojtyniak,<sup>\*,a,b,c</sup> and J. Szade<sup>a,b</sup>Received Date  
Accepted Date

DOI: 10.1039/xxxxxxxxxx

www.rsc.org/journalname

The relation between surface morphology and local conductance was studied for single crystalline thin films of Bi<sub>2</sub>Te<sub>3</sub> grown on mica. Atomic force microscopy and electron diffraction revealed hexagonal order of surface with quintuple layer steps and spiral islands. Furthermore, the experiments using contact mode AFM with conducting tip performed at room temperature has revealed the high conductance of the surface, which was locally reduced due to changes in the local electronic structure at the defects (e.g. edges of the terraces). Contact current-voltage characteristics tested over the surface showed linear behavior in every point, with the resistance significantly lower than the resistance of reference metallic samples (gold, platinum). We show that local conductivity AFM is a good technique to exploit the peculiar surface properties of topological insulators.

In topological insulators (TI), such as Bi<sub>2</sub>Te<sub>3</sub>, the bulk is semiconducting but the surface is highly conductive due to the specific electronic states<sup>1–3</sup>. These surface states are protected against impurities and defects by topology and their spin is locked at right angle to their momentum<sup>4–8</sup>. They are characterized by linear energy dispersion – a Dirac cone is formed in the *k* space. Surface states are very stable and the sheet electrical resistance in the high quality monocrystalline films is characterized by high carrier mobility and surface conductance *G<sub>s</sub>*, which is quantized and reaches the values close to 40 and 25 *e*<sup>2</sup>/*h* for low and high temperatures<sup>9,10</sup>. All of these remarkable properties of TI make them the promising candidates for applications ranging from spintronics to quantum computing<sup>11–14</sup>.

The bulk component of the Bi<sub>2</sub>Te<sub>3</sub> electronic structure is characterized by a narrow energy band gap which value is however given in a broad range depending on the experiment and method of calculations. The value close to 0.16 eV is reported in high quality undoped samples<sup>10</sup>. The Fermi level formed by the surface states is then placed roughly in the middle of the bulk gap. Bi<sub>2</sub>Te<sub>3</sub> crystallizes in the rhombohedral structure belonging to the R3m space group. Most interesting part of the unit cell, which determines its peculiar behavior is the quintuple layer (QL) – a sequence of five atomic layers consisting of covalently bonded *Te*(1) – *Bi* – *Te*(2) – *Bi* – *Te*(1). The QLs are weakly bonded each

together by van der Waals interactions. The thickness of the QL in Bi<sub>2</sub>Te<sub>3</sub> is about 1 nm<sup>15</sup>, while the lattice constant extends for 3 QLs in the [001] direction.

Determination of the surface properties is difficult mainly due to the fact that the bulk conductivity can overwhelm the contribution of the surface states. One of the methods which enables testing predominantly the surface is atomic force microscopy (AFM). Application of one of the AFM modes using the conducting tip allows to measure the local electrical properties and their correlations with the surface topography. Moreover, it allows to measure the local current-voltage characteristics. The distribution of the local resistance and its relation to the details of topography can be a valuable information for models of surface conductivity. It is also an complementary technique to the scanning tunneling microscopy (STM) and scanning tunneling spectroscopy (STS). STM and STS studies have been used to investigate the local density of states proving the basic properties of peculiar surface states including scattering effects<sup>16,17</sup>. However, most results were obtained at low temperatures and STM is not a direct probe of resistance nor surface topography.

In this paper we report the results of microscopic studies of thin Bi<sub>2</sub>Te<sub>3</sub> films. In order to obtain reliable information on the surface topography and conductance we studied single crystalline films of this 3D topological insulator. We used the Molecular Beam Epitaxy (MBE) technique to grow thin Bi<sub>2</sub>Te<sub>3</sub> films on the mica (110) substrates. The surface structure of deposited films was characterized *in situ* by Reflection High-Energy Electron Diffraction (RHEED) and Low-Energy Electron Diffraction (LEED). X-ray Photoelectron Spectroscopy (XPS) was used to confirm purity and stoichiometry. AFM in tapping mode has been used to study the layer growth process with high lateral resolution while the con-

<sup>a</sup>A. Chelkowski Institute of Physics, University of Silesia, Uniwersytecka 4, 40-007 Katowice, Poland

<sup>b</sup>Silesian Center for Education and Interdisciplinary Research, 75 Pułku Piechoty 1A, 41-500 Chorzów, Poland

<sup>c</sup>Institute of Materials Science, University of Silesia, 75 Pułku Piechoty 1A, 41-500 Chorzów, Poland

\*E-mail: marcin.wojtyniak@us.edu.pl

tact mode (LC-AFM) with conducting tip was applied to examine character of the local conductivity at various polarization and bias voltage values. It is worth to mention that our studies were performed at the room temperature. Such tests of the surface properties meet requirements expected for future devices based on TIs.

The  $\text{Bi}_2\text{Te}_3$  films were deposited on the freshly cleaved (110) 0.15-0.17 mm thick Muscovite mica substrate (Ted Pella, Inc.) annealed at 230°C for 1.5 h under UHV conditions ( $5 \cdot 10^{-9}$  mbar). High-purity Bi (99.999% Aldrich Chem. Co.) and spectrographically standardized Te ingots (Johnson Matthey Chemicals) sources were evaporated by conventional effusion Knudsen cells (K-cell) in the co-deposition mode. The K-cell temperatures of Bi and Te were 401 and 206°C respectively, while mica substrate was kept at 130°C. The deposition rates were controlled by the quartz micro balance with growth rate of  $\sim 0.21$  QL/min.

The RHEED measurements of the mica substrate along [110] direction are shown in Fig.1 a). The obtained patterns are slightly diffused (blurred), which results from insulating properties of the substrate. The streaks near the first Laue zone and spots in the second-order Laue zone are characteristic for the crystalline atomically flat surface. Moreover, the Kikuchi pattern suggests that the substrate surface is smooth<sup>18</sup>, which was confirmed by AFM (RMS = 0.9 Å). The spacing between the principal diffraction lines is consistent with a lattice spacing of  $a = 5.21$  Å, which is in good agreement with the reference value<sup>15</sup>.

The typical RHEED image of  $\text{Bi}_2\text{Te}_3$  film shows diffraction pattern along two incident beam directions: [100] and [1 $\bar{2}$ 0]. The pattern (see Fig.1 a)) was reproduced after the rotation of 60° relative to the perpendicular c-axis. The obtained lateral lattice parameters were equal to  $a = 4.41$  and 4.34 Å, where the literature value is equal to 4.38 Å<sup>19,20</sup>.

Subsequently, the samples were tested with the use of LEED for the electron energy of 128.5 eV and 100.5 eV for mica and  $\text{Bi}_2\text{Te}_3$  film respectively. Resulting patterns are shown in the insets to Fig.1 a) and 2 a). The LEED pattern for the  $\text{Bi}_2\text{Te}_3$  shows the hexagonal symmetry confirming the single crystalline form of the film. We did not observe the trigonal symmetry indicating one domain structure as in<sup>10</sup>. It is consistent with the AFM characterization shown below.

Analysis of the XPS survey spectra of  $\text{Bi}_2\text{Te}_3$  films showed no oxygen, carbon nor other contamination even after period of a few days in the vacuum chamber ( $1 \cdot 10^{-9}$  mbar). The chemical states of bismuth and tellurium were obtained from the detailed analysis of the Bi4f and Te3d multiplets (see Fig.1 e). The maxima of the Bi4f<sub>7/2</sub> and Bi4f<sub>5/2</sub> peaks at 157.3 eV and 162.6 eV respectively are in good agreement with the values reported for the  $\text{Bi}_2\text{Te}_3$  single crystal<sup>20,21</sup>. This, in combination with narrow and single component lines, indicates one chemical state corresponding to the  $\text{Bi}_2\text{Te}_3$  compound. The same agreement was found for the Te doublet. Fig.1 e) shows also a fragment of the valence band spectrum in the region of the Fermi energy. The finite density of states at the Fermi level is detected. The smearing of the photoelectron intensity is of about 0.3 eV due to the Gaussian broadening caused mainly by the limit of x-ray monochromatization. The intensity at the Fermi level is thus an indication of metallic states.

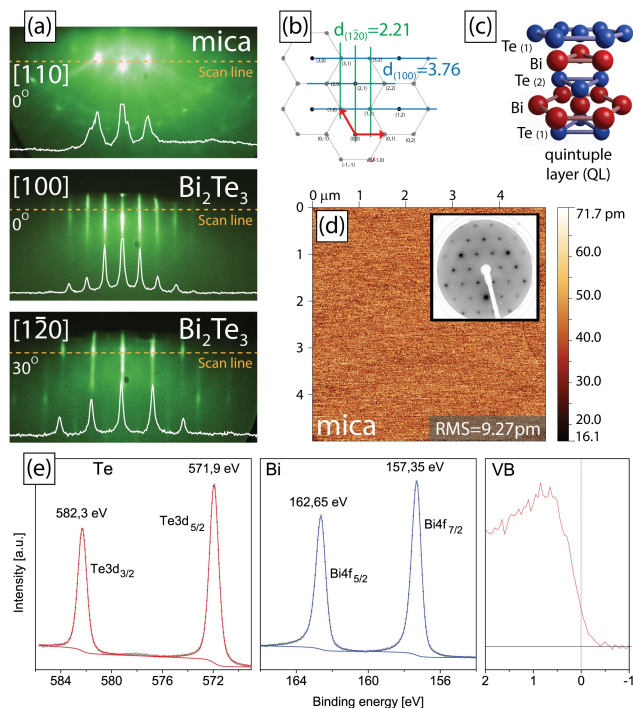


**Fig. 1** a) RHEED patterns for: mica with e-beam aligned along [110] direction (top) and  $\text{Bi}_2\text{Te}_3$  along [100] and [1 $\bar{2}$ 0] directions (middle and bottom); the white line in each figure is the intensity profile along the dashed (orange) scan line, b) structure of surface layer of  $\text{Bi}_2\text{Te}_3$  with the [100] and [1 $\bar{2}$ 0] directions, c) fraction of  $\text{Bi}_2\text{Te}_3$  unit cell showing so called quintuple layer (QL), d) AFM topography and the LEED pattern (inset) of the mica substrate, e) XPS spectra of Bi4f and Te3d core levels and the valence band in the region close to the Fermi level.

The sample topography was measured using separate UHV AFM system, thus the sample was shortly ( $< 5$  min) introduced to the external atmosphere. It was shown that short exposure to the ambient conditions causes only a slight decrease of the surface resistance<sup>10</sup>. The typical surface topography of the air-cleaved mica surface is presented in Fig.1 d). The image of typical  $5 \times 5 \mu\text{m}$  was recorded by non-contact AFM ( $df = -10$  Hz). No visible terraces were found and the average RMS value was found to be in the order of 0.9(1) Å, therefore we conclude that the substrate was atomically flat and did not contribute to the  $\text{Bi}_2\text{Te}_3$  morphology in any way. The typical topography of the obtained  $\text{Bi}_2\text{Te}_3$  films is shown in Fig.2 a) suggesting Stranski-Krastanov like growth<sup>22</sup>. The flat areas constitute relatively small part of the topography. The RMS was found to be of about 9.0(1) Å. The surface is mostly formed of characteristically triangular-shaped islands reflecting the hexagonal crystal structure in the [001] direction. A number of pyramidal-shape terraces with  $\sim 1$  nm high flat steps are visible (topography profile shown in Fig.2 b) along white dashed line in Fig.2 a)). The height distribution presented in Fig.2 c) shows that the distance between the terraces is very close to 1 nm, which is in a good agreement with thickness of a single QL<sup>15</sup>. This behavior is characteristic for the  $\text{Bi}_2\text{Te}_3$  growth, since no atomic-layer by atomic-layer growth was observed, instead the QL by QL growth was found<sup>3,23</sup>. Other TI films, such as  $\text{Bi}_2\text{Se}_3$ , show similar type of growth<sup>24-27</sup>. What is also

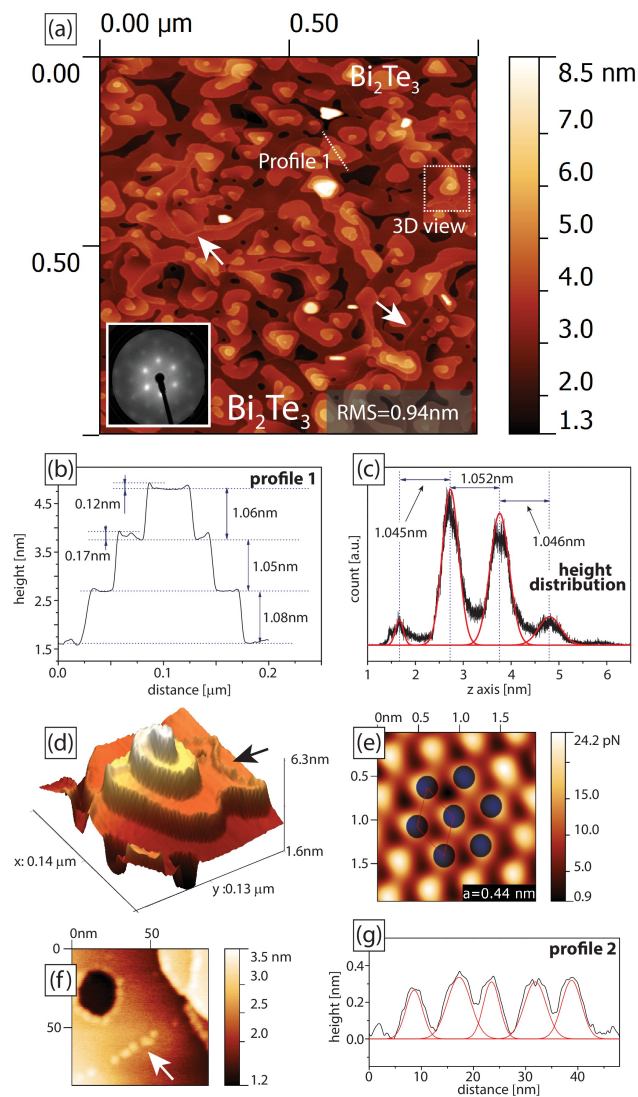


**Fig. 2** a)  $1 \times 1 \mu\text{m}$  non-contact AFM topography obtained for the  $\text{Bi}_2\text{Te}_3$  thin film, b) topography profile along the dashed line visible in a) the height of each step is close to 1 nm, c) the height distribution for the area marked in a), d) the three-dimensional AFM images showing the islands, with characteristic spiral morphology, e) atomic resolution obtained from the lateral force in a contact AFM mode; the interatomic distance was close to  $a=4.4 \text{ \AA}$ , f) non-contact AFM images showing mono-atomic (high) surface inclusions, g) topography profile along the line of small features marked by a white arrow in f).

interesting, is the shape of the observed pyramids suggesting a spiral-like growth, which is well visible in the 3D image shown in Fig.2 d). The height of a spiral step is also very close to the thickness of a single QL, which may suggest that the growth process was close to thermodynamic equilibrium, while the spiral shape results from the dislocations having a screw component. Similar type of surface structure was already observed<sup>28,29</sup>.

We also managed to obtain atomic resolution of  $\text{Bi}_2\text{Te}_3$  thin film surface using the lateral force image shown in Fig.2 e). The hexagonal structure with inter-atomic distance close to  $a=4.4 \text{ \AA}$  was found, which fits well the value obtained from RHEED experiment. The further investigation of the sample topography shown in Fig.2 f) revealed characteristic features - small round shapes that are marked by white arrow. These features are typically located on the edges of the individual layers or at parts of a layer arranged in a single line. The diameter of these agglomerates was estimated from a cross-section presented in Fig.2 g) to be  $1.2 \text{ \AA}$ , however this value can be overvalued due to the profile broadening effect from the tip-sample convolution. The observed structures can be attributed to contaminations or precipitations of one of the elements. The atomic concentration derived from XPS showed a slight excess of Bi. We can thus attribute the observed structures to Bi. The structures do not form large enough objects to give photoemission lines corresponding to pure Bi. We did observe such lines in the polycrystalline films deposited on  $\text{Si}^{30}$ . One has to remember that the investigated sample was exposed for a short time to ambient atmosphere, thus it is possible that observed structure originates from partly ordered tellurium oxide.

Further investigation of the local nature of conductivity of grown  $\text{Bi}_2\text{Te}_3$  thin films involved the use of the LC-AFM technique. In this method a conducting tip is brought in contact with the thin film surface and a small voltage in the range of several mV is applied as depicted in Fig.3 a). Thus, both the local current and the typical AFM topography are simultaneously recorded. This setup allows to track the local changes in the resistance of the surface. Furthermore, the current as a function of the voltage ( $I$ - $V$  curves) can be measured at arbitrary locations. An example of such process is shown in Fig.3 b), where the data from  $500 \times 500 \text{ nm}$  region was gathered. The plot consists of 2500 curves, the red line corresponds to the point with the lowest resistance, while the blue one corresponds to the average value from all curves. The lowest measured resistance corresponded to approximately  $55 \text{ k}\Omega$ . It is worth to mention, that the resistance of the tip, assuming the contact area of about  $1 \text{ nm}^2$ , is of the same order. By comparison, we found higher values of the resistance using similar tip for a noble metal sample. Additionally, our measurement was performed at a very low voltage of few mV, this allows us to believe that LC-AFM method is capable of testing fine variation of the local electronic structure by investigating changes of local conductivity.

While all presented results were obtained with the use of boron-doped diamond coated silicon tip, some measurements using other types of conducting tips, such as the Pt-coated silicon tip, were made. We found no differences in the overall behavior of the topography or the conductivity. Nevertheless, the diamond coated tip was proven to be more stable and the results were more

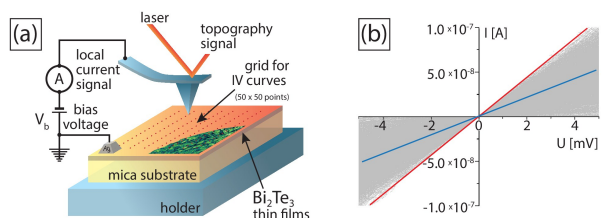


**Fig. 3** LC-AFM measurements: a) LC-AFM techniques scheme b) the I-V grid measurement consisting of  $50 \times 50$  curves at  $\pm 5$  mV voltage; the red line and blue line corresponds to the lowest resistivity and the average resistivity points respectively.

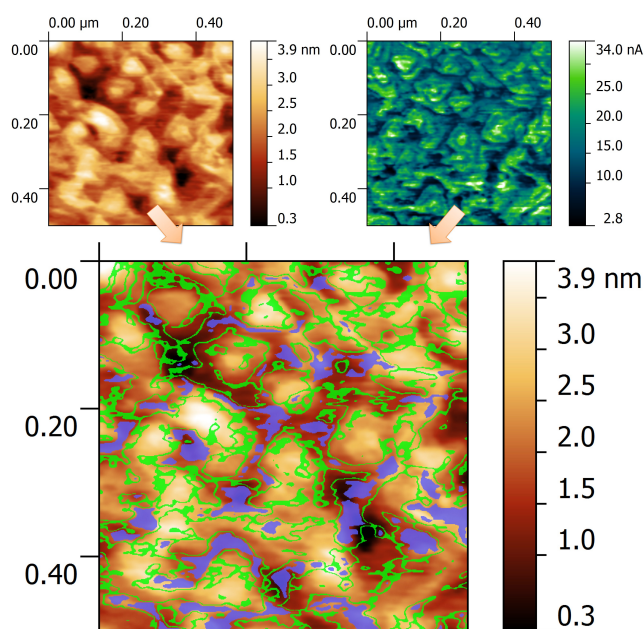


**Fig. 4** LC-AFM measurements carried on  $\text{Bi}_2\text{Te}_3$  thin film in the  $0.5 \times 0.5 \mu\text{m}$  region: a) topography, b) local current map, c) correlation of local current and the topography presented as two colored current masks over topographic image: blue corresponds to 0 to 30 % (0 nA to 5.523 nA) and green corresponds to 42 to 52 % (7.732 nA to 9.573 nA) range.

reproducible.

The obtained surface topography presented in Fig.4 a) exhibited similar features as observed in good resolution NC-AFM image (Fig.2 a)). The RMS for the  $0.5 \times 0.5 \mu\text{m}$  scanning area was equal to  $5.88 \text{ \AA}$ . The local current map can be seen in the Fig.4 b). The average current value was equal to 18.41 nA for 5 mV voltage bias. The correlation between the local current map and the topography was made in a form of two different current masks overlapped on the topography image - Fig.4 c). The blue colored mask correspond to the area, where the current value was in the range of 0 - 30 % of the maximum, while the green correspond to the range of 42 to 52 %. Those specific ranges were selected in order to mark the differences in the electrical behavior of the thin film surface. For example, the top of triangular islands (Fig.3 a)) conducts well, while the areas under the green mask exhibits lower conductivity. Typically, a correlation between the topography and the current map is related to the differences in the tip-surface contact during measurement. When the lateral force is applied to

the tip due to friction (fast scan direction), the tip-sample contact area increases leading to an increase of the measured current. This effect should be also visible at topographical features as an increase in the current when a tip contacts a higher feature, and as a decrease in current when a tip overcomes the feature. The opposite behavior should be found with the change of scanning direction. However, in this case, no differences upon the direction of the scan (left-right) were found. Instead a reverse behavior, the decrease of the current on the terrace edges was detected.

Therefore, we believe that such decrease in the conductivity can originate only from the changes in the surface electronic state. The Alpishev et al.<sup>31</sup> studied the vicinity of the topographical step using the STM and found one-dimensional bound state that runs parallel to the step edge. What is more, the Biswas et al.<sup>32</sup> showed that Dirac fermions existing in the topological insulator surface can be trapped by potential barriers such as impurities. Such impurity-induced Dirac state suppression was even found at certain distance ( $\sim 2 \text{ \AA}$ ) from the defect<sup>29</sup>. Therefore, the topological step-induced Dirac state suppression could explain the observed decrease in the surface conductivity.

On the other hand, the decreased current in the regions under the blue colored mask can be attributed to the surface contamination. This contamination originates from the short time exposure to ambient condition. Typically, the short exposure of  $\text{Bi}_2\text{Te}_3$  to air caused a slight decrease of the sheet resistance as investigated by Hofer et al.<sup>10</sup>. They have shown, that the surface adsorbates caused shift of the Fermi level and increase of the charge carriers concentration due to band bending effect. They also calculated, that after 5 min exposure, the density of contaminants left adsorbed was in the order of several  $10^{12} \text{ cm}^{-2}$ . However, this is only a small fraction of the full coverage possible, which is in the order of  $10^{14} \sim 10^{15} \text{ cm}^{-2}$  under ambient conditions. Such surface contamination is not likely to be homogeneous, and is limited to the small percentage of the surface. Thus, due to the well known effect of the decrease of the electric field under the AFM tip in the presence of the contamination (adsorbate) layer<sup>33</sup>, we observe artificial decrease of the LC-AFM current.

In conclusion, we showed room temperature characterization of the  $\text{Bi}_2\text{Te}_3$  thin films grown on mica. The electron diffraction showed monocrystalline structure of the films. The Stranski-Krastanov like growth was found with the presence of screw islands, which most probably, were formed due-to to the film-substrate mismatch. The terraces detected via AFM had the height of one quintuple layer. XPS confirmed pure chemical state of the compound components. However, we detected precipitations on the surface located mainly at the edges of terraces. We ascribe them to the excess of Bi found in atomic composition derived from the XPS data. Application of LC-AFM allowed to show extremely high conductivity (very high contact currents) and metallic behavior (linear I-V curves) of  $\text{Bi}_2\text{Te}_3$  films surface, which most likely is an effect of the presence of the Dirac surface states. At the same time, we were able to localize small regions with reduced conductance, which were attributed to the local changes of the electronic structure caused by various defects: add-atoms, terrace edges, steps, etc.

One of the authors R.R. is grateful for the support from the

Forszt project co-financed by EU from the European Social Fund.

## Literatura

- 1 Y. -Y. Li, G. Wang, X. -G. Zhu, M. -H. Liu, C. Ye, X. Chen, Y. -Y. Wang, K. He, L. -L. Wang, X. -C. Ma, H. -J. Zhang, X. Dai, Z. Fang, X. -C. Xie, Y. Liu, X. -L. Qi, J. -F. Jia, S. -C. Zhang, and Q. -K. Xue, *Adv. Mater.*, 2010, **22**, 4002–4007.
- 2 G. Wang, X. -G. Zhu, Y. -Y. Sun, Y. -Y. Li, T. Zhang, J. Wen, X. Chen, K. He, L. -L. Wang, X. -C. Ma, J. -F. Jia, S. B. Zhang, and Q. -K. Xue, *Adv. Mater.*, 2011, **23**, 2929–2932.
- 3 J. Krumrain, G. Mussler, S. Borisova, T. Stoica, L. Plucinski, C.M. Schneider, D. Grutzmacher, *J. Cryst. Growth*, 2011, **324**, 115.
- 4 C. L. Kane and E. J. Mele, *Phys. Rev. Lett.*, 2005, **95**, 146802.
- 5 C. L. Kane and E. J. Mele, *Phys. Rev. Lett.*, 2005, **95**, 226801.
- 6 B.A Berneving, T.L Hughes, S. -C Zhang, *Science*, 2006, **314**, 1757.
- 7 L. Fu, C. L. Kane, and E. J. Mele, *Phys. Rev. Lett.*, 2007, **98**, 106803–1.
- 8 L. Fu, and C. L. Kane, *Physical Review B*, 2007, **76**, 045302–1.
- 9 P. Ghaemi, R. S. K. Mong and J. E. Moore, *Phys. Rev. Lett.*, 2010, **105**, year.
- 10 K. Hofer, C. Becker, D. Rata, J. Swanson, P. Thalmeier, and L. H. Tjeng, *Proc. Natl. Acad. Sci. U.S.A.*, 2014, **111**, 14979–84.
- 11 H. Peng, W. Dang, J. C., Y. Chen, D. Wu, W. Zheng, H. Li, Z. -X. Shen, Z. Liu, *Nat. Chem.*, 2012, **4**, 281.
- 12 L. Jiang, C. L. Kane and J. Preskill, *Phys. Rev. Lett.*, 2011, **106**, 0504.
- 13 J. Linder, Y. Tanaka, T. Yokoyama, A. Sudbo, N. Nagaosa, *Phys. Rev. Lett.*, 2010, **104**, 067001.
- 14 M. Z. Hasan and C. L. Kane, *Rev. Mod. Phys.*, 2010, **82**, 3045.
- 15 W. de Poel, S. Pinteá, J. Drnec, F. Carla, R. Felici, P. Mulder, J. A.A.W. Elemans, W. J.P. van Enckevort, A. E. Rowan, E. Vlieg, *Surf. Sci.*, 2014, **619**, 19–24.
- 16 W. Ko, I. Jeon, H. W. Kim, H. Kwon, S. -J. Kahng, J. Park, J. S. Kim, S. W. Hwang, H. Suh, *Sci Rep*, 2013, **3**, 1–5.
- 17 P. Cheng, T. Zhang, K. He, X. Chen, X. Ma, Q. Xue, *Phys E*, 2012, **44**, 912–916.
- 18 Y. Iwata, H. Kobayashi, S. Kikuchi, E. Hatta , K. Mukasa, *J. Cryst. Growth*, 1999, **203**, 125–130.
- 19 R. Sathyamoorthy, J. Dheepa, *J. Phys. Chem. Solids*, 2007, **68**, 111–117.
- 20 I. V. Gasenkova, M. K. Zhitinskaya, S. A. Nemovet, T. E. Svehnikova, *Phys. Solid State*, 1999, **41**, 1805–1808.
- 21 H. Bando, K. Koizumi, Y. Oikawa, K. Daikohara, V. A. Kulbachinskii and H. Ozaki, *J. Phys.: Condens. Matter*, 2000, **12**, 5607–5616.
- 22 J. A. Venables, *Introduction to Surface and Thin Film Processes*, Cambridge University Press, 2000.
- 23 K. Wang, Y. Liu, W. Wang, N. Meyer, L. H. Bao, L. He, M. R. Lang, Z. G. Chen, X. Y. Che, K. Post, J. Zou, D. N. Basov, K. L. Wang, and F. Xiu, *Appl. Phys. Lett.*, 2013, **103**, 031605.
- 24 M.L. Teague, H. Chu, F.-X. Xiu, L. He, K.-L. Wang, N.-C. Yeh, *Solid State Commun.*, 2012, **152**, 747–751.
- 25 C. Klein, M. Vyshnepolsky, A. Kompch, F. Klasing, A. Hanisch-Blicharski, M. Winterer, M. Horn-von Hoegen, *Thin Solid Films*, 2014.
- 26 X. Liu, D.J. Smith, H. Cao, Y. P. Chen, J. Fan, Y. -H. Zhang, R. E. Pimpinella, M. Dobrowolska, J. Furdyna, *Journal of Vacuum Science and Technology B*, 2012, **30**, year.
- 27 Z.Y. Wang, H.D. Li, X. Gu, W.K. Ho, M.H. Xie, *J. Cryst. Growth*, 2011, **334**, 96–102.
- 28 M. Ferhat, J. -C. Tedenac , J. Nagao, *J. Cryst. Growth*, 2000, **218**, 250–258.
- 29 M. L. Teague, H. Chu, F. -X. Xiu, L. He, K. -L. Wang, and N. -C. Yeh, *Solid State Commun.*, 2012, **152**, 747–751.
- 30 R. Rapacz, K. Balin, A. Nowak, J. Szade, *J. Cryst. Growth*, 2014, **401**, 567–572.
- 31 Z. Alpichshev, J. G. Analytis, J. -H. Chu, I. R. Fisher, and A. Kapitulnik, *Phys. Rev. B*, 2011, **84**, 1–5.
- 32 R. R. Biswas, A. V. Balatsky, *Phys. Rev. B*, 2010, **81**, 233405.
- 33 F. Peter, A. Rüdiger, R. Dittmann, R. Waser, K. Szot, B. Reichenberg, K. Prume, *Appl. Phys. Lett.*, 2005, **87**, 1–3.